

# Exploration on Unsteady and Transient Combustion Phenomena in High-Speed Air-Breathing Propulsion

Kuo-Cheng Lin  
Taitech, Inc.  
Beavercreek, Ohio, U.S.A.

Vigor Yang  
Georgia Institute of Technology  
Atlanta, Georgia, U.S.A.

## 1 Introduction

Flame stabilization and combustion transients during flame ignition have been a serious concern in the development of high-speed air-breathing engines due to the difficulties to anchor stable flames in a high-speed environment. The situation becomes even more challenging during the engine start-up stage at which the low chamber pressure and unsettled fuel/air mixing tend to blow out the flame, even when a flame holding device such as a cavity is employed. At a low flight Mach number, however, combustion may take place in subsonic regions, such as boundary layers, recirculation zones in flame-holding devices, or the region behind the pre-combustion shock train at the dual mode combustion. The resultant heat release then causes the flow to accelerate to a supersonic state in the downstream section of the divergent combustor [1]. During this process, a longitudinal mode of thermoacoustic instability may develop in a spatial domain reaching from the shock train in to the combustion zone.

The present work investigates, both experimentally and analytically, thermoacoustic instabilities inside an ethylene-fueled supersonic combustor with a recessed cavity flameholder. High-speed pressure transducers, positioned at the base and downstream of the cavity flameholder, are utilized to record acoustic signals under various flow conditions and flameholder geometries. The effects of fuel/air equivalence ratio, fueling scheme, and simulated flight conditions on the stability characteristics of the combustor are examined systematically. The measured acoustic oscillation frequencies and the corresponding amplitudes are used to explore the underlying flow physics. In addition, the present measurements are compared with existing acoustic data for different combustor flowpaths to help identify the mechanisms responsible for driving and sustaining combustion oscillations. The present work also attempts to establish an integrated theoretical/numerical framework within which the influences of all known effects (including the location and operating timing of air throttling and fuel injection) on the engine ignition transient and flame development can be studied systematically. The basis of the work is an integrated three-dimensional numerical analysis capable of treating detailed combustion dynamics in realistic engine environments. The physical model simulates the experimental facility operated at the Air Force Research Laboratory.

## 2 Experimental Methods

The experiment effort was carried out on the thrust stand inside Research Cell 18 at the Wright-Patterson Air Force Base. This facility was designed for fundamental studies of supersonic reacting flows using the continuous-run direct-connect open-loop air flow. The entire test rig consists of a vitiator, facility nozzle, modular isolator, modular combustor, and exhaust pipe, as illustrated in Fig. 1. With the currently available Mach-1.8 and 2.2 facility nozzles, the vitiator was fine-tuned to simulate flight conditions from Mach 3.5 to 5 at flight dynamic pressures of up to 2000 psf (0.943 atm). The relatively low simulated flight Mach numbers represent the scramjet takeover conditions, where the ignition, flame development, flow transients, and combustion stabilization take place. The flowpath in the present study consists of a heat-sink rectangular isolator and a rectangular combustor. The schematic in Fig. 2 shows the flowpath with key combustor features identified. The isolator used in this study has a rectangular cross-sectional area with a height of 1.5 in (38.1 mm), a width of 4.0 in (101.6 mm), and a length of 25.75 in (654.0 mm). The combustor has a total length of 36 in (914.4 mm) and a constant divergence angle of 2.6 degrees. The interior surface of the combustor was covered with either heat-sink or water-cooling panels.

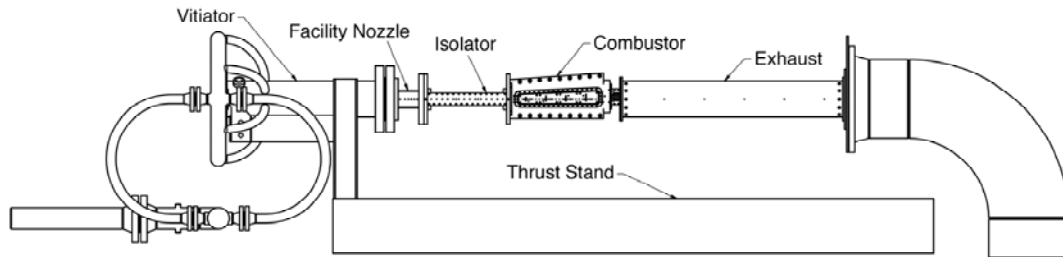
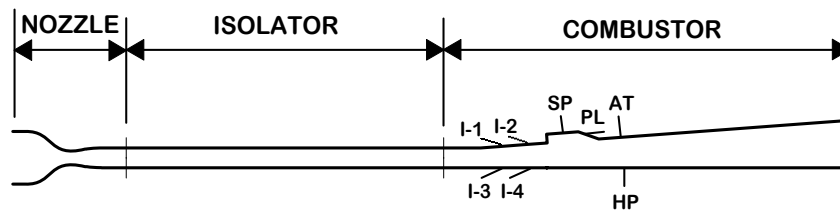


Figure 1. Schematic of Research Cell 18 combustion facility at WPAFB.



- AT Air throttle
- HP High-speed pressure transducer
- I-1 Body side first row 15-degree gaseous injectors
- I-2 Body side second row 15-degree gaseous injectors
- I-3 Cowl side first row 15-degree gaseous injectors
- I-4 Cowl side second row 15-degree gaseous injectors
- PL Pilot fuel injectors
- SP Spark plugs

Figure 2. Schematic of the combustor flowpath and key interior features.

A recessed cavity flameholder is located at the divergent top wall, which is designated as the body side of the scramjet-powered vehicle. The flameholder spans the entire flowpath width and has a forward-facing ramp. Two conventional spark plugs, located at the base of the cavity, were used as the baseline ignition source. In the present study, a high-speed pressure transducer was installed downstream of the cavity flameholder. Four banks of gaseous fuel injectors, two banks each on the top (body) and bottom (cowl) walls, were designed to provide various fueling options. There are 4 orifices on each body-side injection site and 3 orifices on each cowl-side injection site. The design for each gaseous fuel injector features a small-angle flush-wall plain orifice. Pressure taps and thermocouple ports were strategically positioned throughout the entire rig for instrumentation and health monitoring. A high-speed pressure

transducer (100 mV/psi sensitivity, Model 112A22, PCB Group, Inc.) with a signal conditioner (Model 482A20, PCB Group, Inc.) was used to identify acoustic characteristics inside the combustor.

### 3 Numerical Approaches

The physical model of concern includes the entire flowpath shown in Fig. 2, spanning from the entrance of the facility nozzle to the exit of the exhaust nozzle. The theoretical formulation is based on the complete conservation equations of mass, momentum, energy, and species transport in three dimensions. The analysis also accommodates finite-rate chemical kinetics and variable thermophysical properties for a multi-component chemically reacting flow. The two-step global kinetics scheme proposed by Westbrook and Dryer [3] is adopted in light of its simplicity and reasonably accurate modeling of the burned gas containing incompletely oxidized species of hydrocarbon fuels. Turbulence closure is achieved by means of Menter's shear stress transport (SST) model calibrated for high-speed compressible flows [4]. The model incorporates the standard  $k-\varepsilon$  model that is suitable for shear-layer flows and the Wilcox  $k-\omega$  model [5] for wall turbulence effects. To save computational cost and expediate calculations, the wall-function concept proposed by Launder and Spalding [6] is implemented.

The theoretical formulation is treated numerically using a finite-volume approach. The convective fluxes are evaluated by means of Roe's FDS (flux-differencing splitting) method derived for multi-species reacting flows. The MUSCL (monotone upwind schemes for conservation laws) approach is employed for high-order spatial accuracy, along with a minmod slope limiter for the TVD (total variation diminishing) properties. Such a spatial discretization strategy satisfies the TVD conditions and features a high-resolution shock capturing capability. The discretized equations are temporally integrated using a four-stage Runge-Kutta scheme. Further efficiency is achieved with the implementation of a parallel computing technique based on the message-passing-interface (MPI) library. The computational domain, which covers the entire internal flow path spanning from the entrance of the facility nozzle to the exit of the exhaust nozzle, is discretized into  $375 \times 47 \times 44$  grid cells, of which  $50 \times 47 \times 44$  cells are in the cavity. The entire domain is divided into 45 blocks for parallel computing.

## 4 Results and Discussion

### 4.1 Thermoacoustic Instability

Combustion oscillations in subsonic regions of a scramjet combustor can be a major problem for scramjet development. These subsonic regions include boundary layers, recirculation zones associated with flameholders, and an extended region between the pre-combustion shock train and the heat release zone for a scramjet combustor operating in dual mode. A low-frequency, high-amplitude pressure oscillation within these subsonic regions may deteriorate combustion efficiency or even extinguish the flame.

Figure 3(a) illustrates the measured power spectra for injection schemes using the I-2 injection site with others at the same fuel equivalence ratio. The simulated flight condition has a Mach number of 4.5 and a dynamic pressure of 500 psf (0.236 atm). Pressure oscillations with a dominant frequency of 368 Hz were observed for the I-2 only injection scheme. This dominant frequency is similar to the frequency reported by Ma et al. [2] for an ethylene-fueled scramjet combustor with a larger flowpath. This frequency was overtaken by a smaller frequency in the range of 120-140 Hz when a 60/40 fuel split was introduced. The shift of the dominant frequency toward a lower frequency may signal reduced combustor performance for the injection scheme with fuel split.

The shift in the dominant frequency can also be observed for injection schemes using the I-1 injection site with and without I-3, as shown in Fig. 3(b). As the cowl-side injection is introduced, the dominant

frequency shifts from 376 Hz for the I-1 only injection to 120-140 Hz for the fueling schemes with 60/40 fuel split. With the I-1 only injection, the amplitude of the dominant pressure oscillation is significantly higher than that of the I-2 only injection scheme, at a similar fuel equivalence ratio, as shown in Fig. 3(a). Also, a second pressure oscillation with a frequency of 252 Hz, which may be the harmonic mode of the 120-140 Hz pressure oscillation, stands out for the (I-1/I-3) injection scheme in Fig. 3(b).

Figures 3(c) and 3(d) show the power spectra of the detected pressure oscillation as the overall fuel equivalence ratio increases from 0.6 in Fig. 3(a) to 0.8 in Fig. 3(b). Interestingly, the 120-140 Hz pressure oscillation for the injection schemes with 60/40 fuel split becomes insignificant as the equivalence ratio increases. Instead, pressure oscillations with smaller amplitudes and frequencies in the range of 240-290 Hz dominate the injection schemes with fuel split. The body-side only injection schemes still produce similar pressure oscillations even with an increase in the fuel equivalence ratio. Generally, the I-2 only injection scheme generates relatively stable combustion for the conditions shown in Fig. 3.

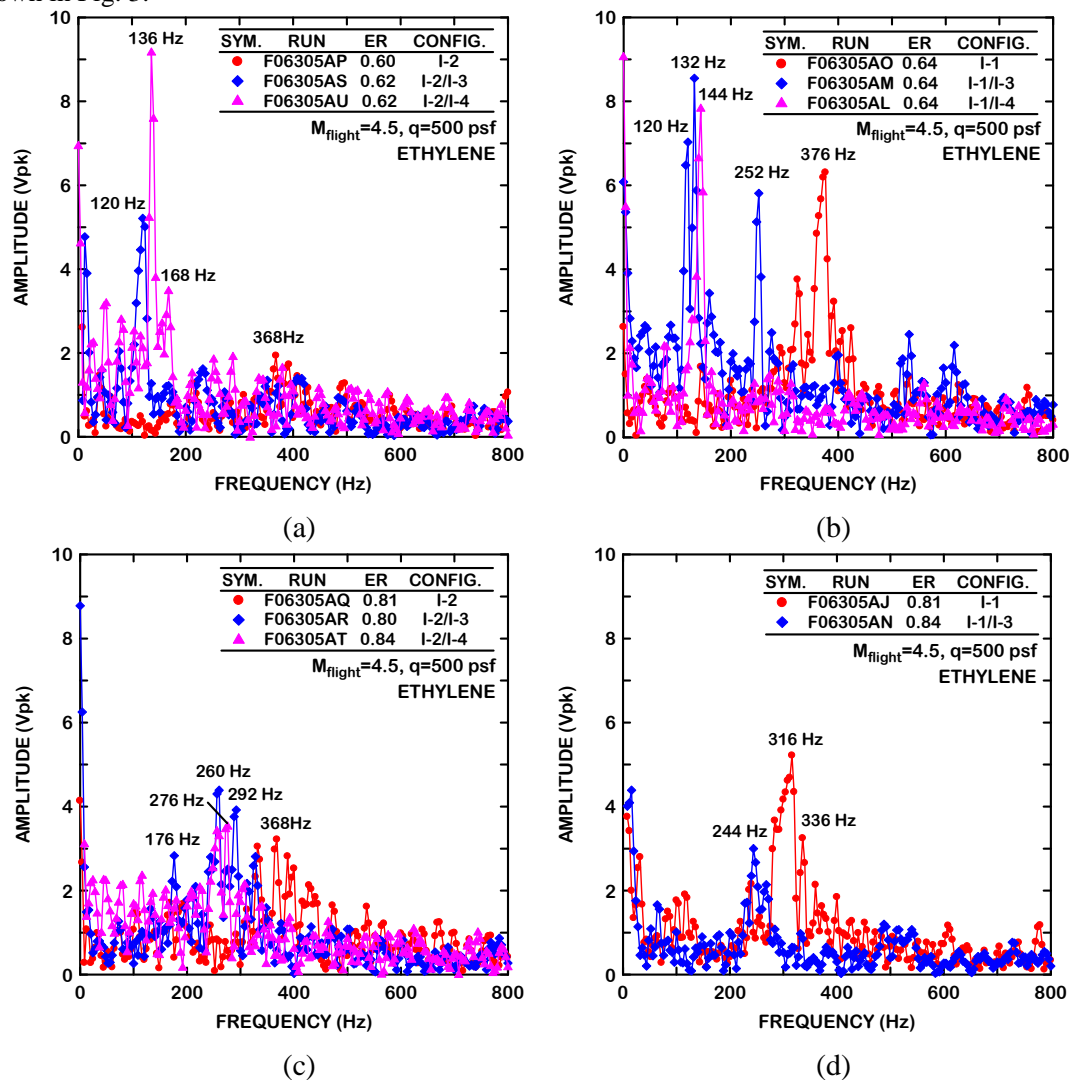


Figure 3. Power spectra of pressure oscillations for various fueling schemes and fuel equivalence ratios;  $M_{flight}=4.5, q=500 \text{ psf}$ .

#### 4.2 Mechanisms of Combustion Oscillations

To understand the underlying mechanisms responsible for driving and sustaining the observed flow oscillations, we first consider the various feedback loops in the subsonic region bounded by the precombustion shock in the isolator and the thermal throat in the downstream region of the flame zone. No such acoustic feedback may exist in a supersonic regime. Two prospective mechanisms are identified: interactions between the precombustion shock and flame zone, and interactions between the fuel injection and flame zone, as illustrated schematically in Fig. 4.

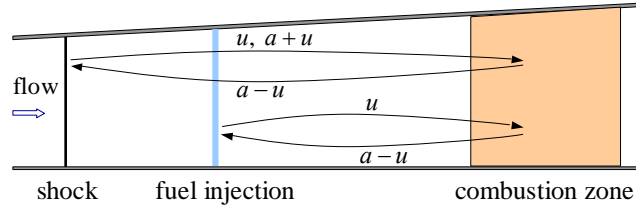


Figure 4. Schematic of acoustic-convective feedback loops in scramjet combustor.

The first mechanism involves the response of the shock wave to flow disturbances arising from the flame zone. Any acoustic wave generated by the heat-release fluctuation in the flame zone can propagate upstream to the shock wave, bounces back, and then travels downstream to interact with the flame. The characteristic time can be calculated as

$$\tau_{sf} = \int_{x_s}^{x_f} \frac{dx}{a-u} + \int_{x_s}^{x_f} \frac{dx}{a+u} \approx \frac{L_{sf}}{\bar{a}-\bar{u}} + \frac{L_{sf}}{\bar{a}+\bar{u}} = \frac{2L_{sf}}{\bar{a}(1-\bar{M}^2)} \quad \text{i.}$$

with  $\bar{a}$  and  $\bar{M}$  representing the speed of sound and Mach number longitudinally averaged between the shock and flame, respectively, and  $x_s$  and  $x_f$  the locations of the shock and flame, respectively.

The second mechanism is associated with the acoustic-convective interactions in the region between the fuel injection and the flame zone. The acoustic wave generated in the flame zone propagates upstream and alters the fuel distribution when traveling through the fuel injection and mixing zone. If the fuel injection rate is fixed (such as that with a choked injection), the composition and the equivalence ratio of the fuel/air mixture then fluctuates due to the oscillation of the local air mass flow rate and variation of the fuel distribution. The fluctuating fuel/air composition is then convected downstream and causes a heat-release fluctuation in the flame zone, which in turn produces acoustic waves propagating upstream. A feedback loop for driving flow oscillations thus forms. The corresponding characteristic frequency for the acoustic-convective feedback loop between the fuel injection and flame zone becomes

$$f_{if} = n / \tau_{if} \approx \frac{nL_{if}}{\bar{a}-\bar{u}} + \frac{nL_{if}}{\bar{u}} = \frac{nL_{if}}{\bar{a}\bar{M}(1-\bar{M})}, \quad n=1, 2, 3, \dots \quad \text{ii.}$$

with  $\bar{a}$  and  $\bar{M}$  representing the speed of sound and Mach number longitudinally averaged between the shock and flame, respectively, and  $x_s$  and  $x_f$  the locations of the shock and flame, respectively.

The above analysis is applied to explain the oscillation frequencies obtained from various experimental cases. Figure 5 shows the experimentally measured and analytically predicted oscillation frequencies. Nearly all the measured oscillation frequencies fall within the range between the shock-flame feedback frequency ( $f_{sf}$ ) and the injector-flame feedback frequency ( $f_{if}$ ). The two instability mechanisms are observed in most experiments, and the corresponding frequencies match the predictions reasonably well.

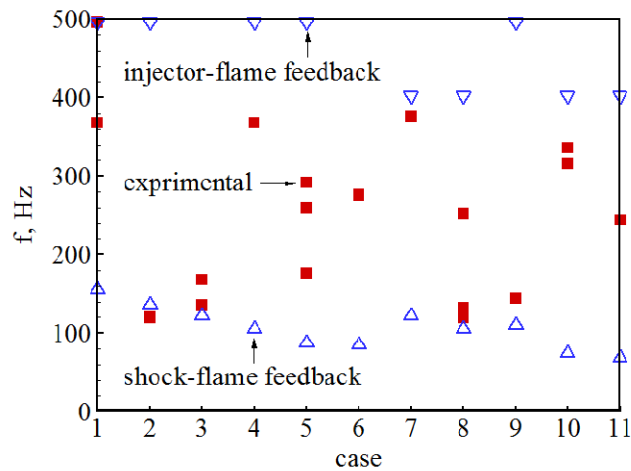


Figure 5. Flow oscillation frequencies from experimental measurements and analytical predictions based on various feedback loops.

Table 1. Typical flow conditions at isolator entrance

Case	Mach number	Axial velocity (m/s)	Static pressure (atm)	Static temperature (K)	Equivalence ratio	$\dot{m}_{air}$ (kg/s)	$\dot{m}_{throttle}$ (kg/s)
1	2.2	1045	0.328	560	0.6	0.757	0.0
2	2.2	1045	0.328	560	0.6	0.757	0.151

### 4.3 Combustion Transients

Calculations are conducted for ignition of the fuel-air mixture in the modeled combustor, based on the simulated steady ethylene injection and air throttling flow field established previously. The inlet conditions and air throttling mass flow rate are provided in Table 1. Stable air throttling is introduced at the axial location  $x=1.36$  m downstream of the cavity at the beginning of the calculation, exactly when ignition of the ethylene/air mixture in the cavity is initiated by a hot-spot igniter at the cavity ceiling. Figure 6 shows the ignition transient and combustion development in the combustor, where iso-surfaces of temperature at  $T=2400 \sim 2800$  K illustrate the flame position. Figure 6(a) indicates that combustion first occurs around the hot-spot igniter at  $t=1.121$  ms, the iso-surfaces of temperature outlining the region of flame. The initiated flame spreads out of the cavity rear ramp in a short time ( $t=1.501$  ms), as seen in Fig. 6(b). Streamwise flow convection near the wall is mainly responsible for the flame propagation downstream. Fig. 6(c) shows that the flame front reaches the slits of the air throttle at  $t=1.930$  ms with a velocity of about 300 m/s within the boundary layer. Benefiting from the significant reduction in velocity in the boundary layer, the reacting flow spreads upstream across the cavity to reach the fuel injection locations on the body surface. In Figures 6(d) to 6(f) the observing angle is lifted to describe the spontaneous ignition and combustion development of the fuel-air mixture on the cowl-side wall of the combustor. The reacting flow begins from individual flame plumes near the fuel injectors on the body-side wall, which interact and merge with each other over the cavity, as shown in Fig. 6(d) at  $t=2.126$  ms. The flame propagates upstream and downstream within the low-momentum boundary layer. Meanwhile on the cowl-side wall, the first sequential ignition of the fuel-air mixture is initiated near the corner. As shown in Fig. 6(e), another sequential ignition at the center region occurs following the spatial flame spreading downstream at  $t=3.015$  ms. The air throttle is turned off right after the flame is anchored near the ethylene injectors on the cowl-side wall, allowing the reacting flow to fully develop through the combustor nozzle. Figure 6(f) demonstrates the

establishment of reacting flow at the end of the calculation ( $t=9.595$  ms). Stable combustion is sustained successfully in the modeled combustor.

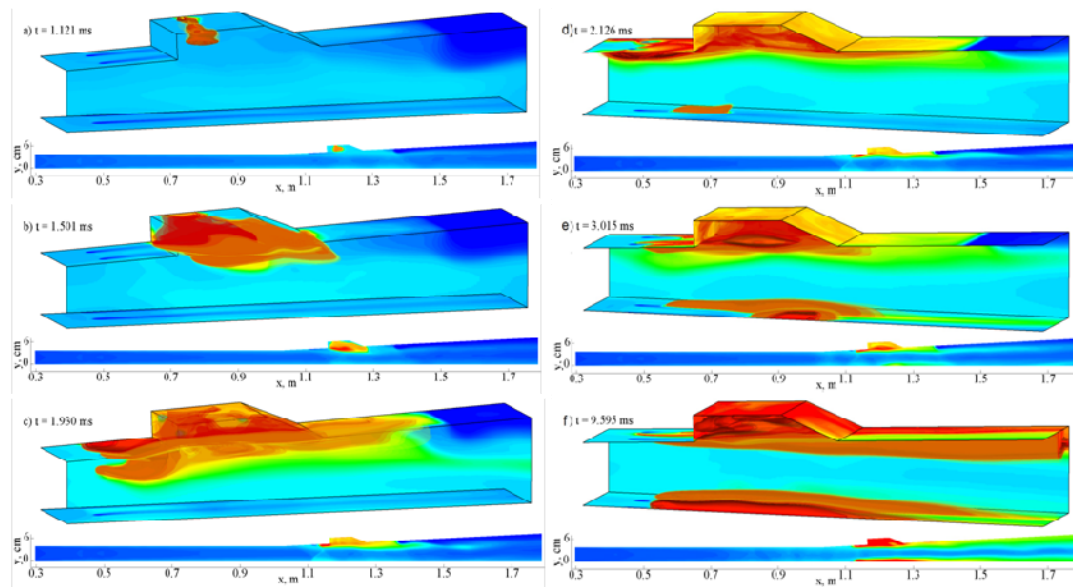


Figure 6. Evolution of the temperature field in the cavity region during the ignition transient on the body-side wall with air throttling ( $\dot{m}_{throttle} = 20\% \dot{m}_{air}$ ).

Figure 7 presents the ignition transient and the time evolution of the flow structures in the combustor in terms of shadowgraph images. The fuel-air mixture in the cavity is ignited by the hot-spot igniter 1.121 ms after the fuel injectors are activated. The initiated flame is clearly illustrated by the shadowgraph image on the x-y plane ( $z/W=3/8$ ), as shown in Fig. 7(a). The reacting flow rises rapidly and develops over the cavity in the combustor in a short time. As the shadowgraph image in Fig. 7(b) shows, the flame is anchored at the cavity and spreads downstream along the low-momentum boundary layer. Heat release from combustion induces local pressure rise and the resultant boundary layer separation leads to spontaneous formation of upstream oblique shock waves. Figure 7(c) presents that at time 4.511 ms: the fuel-air mixture on the cowl surface is ignited, and the reacting flow starts to develop intensively in the modeled combustor. As a result of the combustor pressure rise, the flow separation moves upstream, subsequently the shock waves are pushed into the constant cross-sectional area isolator. When the air throttling is turned off, at this point the reacting flow is sustained in the combustor as seen in Fig. 7(d) (at time  $t=5.963$  ms). Figure 7(e) shows that at  $t=9.557$  ms, a steady pre-combustion shock train is established in the flow field in the constant cross-section area isolator.

## 5 Summary

The thermoacoustic instabilities inside an ethylene-fueled scramjet combustor with a recessed cavity flameholder were investigated both experimentally and analytically. Pressure oscillations with frequencies of 100-500 Hz inside the flowpath were measured and identified. The observed phenomena may be attributed to the acoustic feedback loop between the shock and flame zone, and to the acoustic-convective feedback loop between the fuel injection and flame zone. The effects of the throttling air flow on ignition enhancement and flameholding were analyzed. Air throttling generates a pre-combustion shock train in the isolator. More detailed discussion will be presented at the final paper.

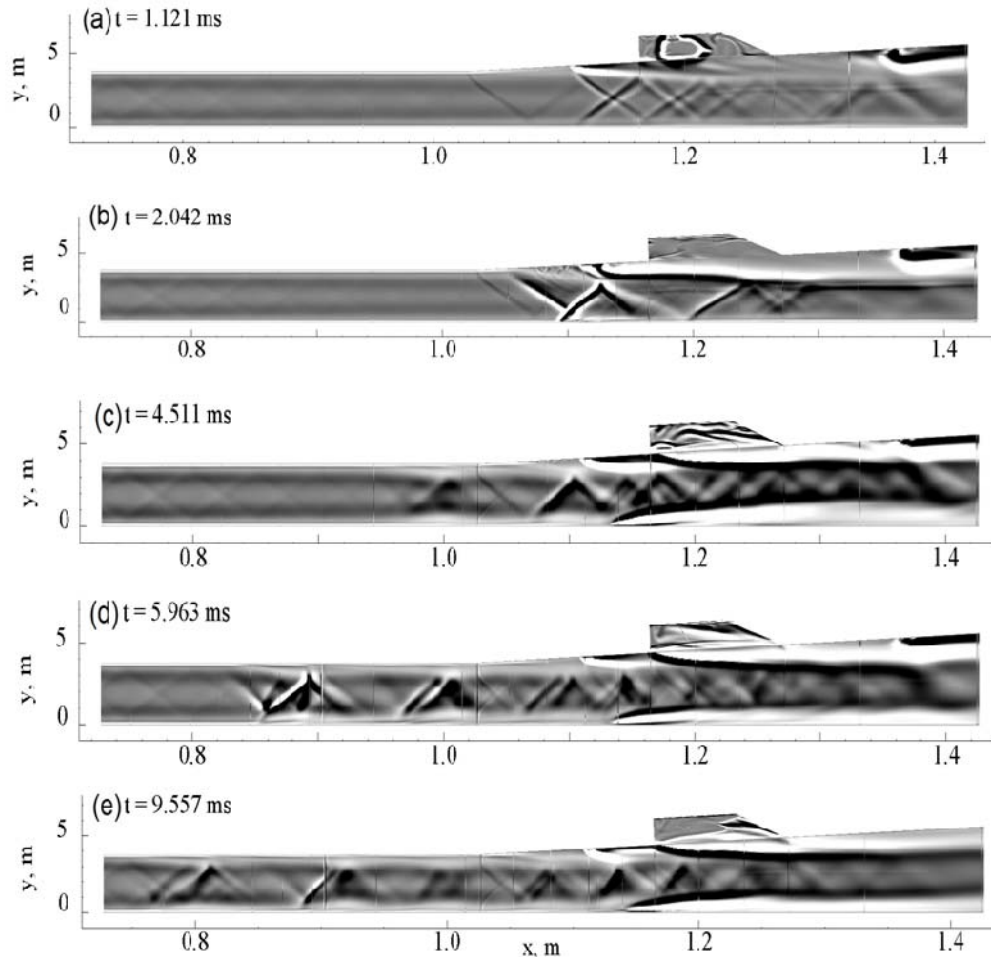


Figure 7. Evolution shadowgraphs during the ignition transient with air throttling ( $\dot{m}_{throttle} = 20\% \dot{m}_{air}$ )

## 6 Acknowledgement

This work was sponsored by the AFRL/Propulsion Directorate under contract number FA8650-08-D-2844 (Contract monitor: Stephen Smith). Assistance from the air facility group of the Air Force Research Laboratory is acknowledged. Also, the authors would like to thank Paul Kennedy (AFRL/RZAS), Matt Streby, Steve Enneking (Taitech, Inc.), Jian Li, and Fuhua Ma (The Pennsylvania State University) for their contributions in hardware design, setup, rig operation, data acquisition, and numerical execution.

## References

- [1] Choi, J. Y., Ma, F. H., and Yang, V., "Combustion Oscillations in a Scramjet Engine Combustor with Transverse Fuel Injection," *Proceedings of the Combustion Institute*, Vol. 30, No. 2, 2005, pp. 2851-2858.
- [2] Ma, F. H., Yang, V., Li, J., Lin, K. C., and Jackson, T. A., "Thermoacoustic Flow Instability in a Scramjet Combustor," AIAA Paper 2005-3824, July 2005.

- [3] Westbrook, C. K. and Dryer, F. L., "Simplified Reaction Mechanisms for the Oxidation of Hydrocarbon Fuels in Flames," *Combustion Science and Technology*, Vol. 27, 1981, pp. 31-43.
- [4] Menter, F. R., "Two-equation eddy-viscosity turbulence models for engineering applications," *AIAA Journal*, Vol. 32, No. 8, 1994, pp. 1598-1605.
- [5] Wilcox, D. C., *Turbulence Modeling for CFD*, DCW Industries, La Cañada, CA, 1993.
- [6] Launder B. E., Spalding D. B., *Mathematical Models of Turbulence*, 1972, Academic Press.